Design and Performance of an Adaptive Low-DC-Voltage-Controlled LC-Hybrid Active Power Filter With a Neutral Inductor in Three-Phase Four-Wire Power Systems

Chi-Seng Lam, *Member, IEEE*, Man-Chung Wong, *Senior Member, IEEE*, Wai-Hei Choi, *Student Member, IEEE*, Xiao-Xi Cui, Hong-Ming Mei, and Jian-Zheng Liu

***Abstract*—This paper proposes an adaptive low-dc-link-voltage-controlled LC coupling hybrid active power filter (LC-HAPF) with a neutral inductor, which can compensate both dynamic reactive power and current harmonics in three-phase four-wire distribution power systems. Due to its adaptive low-dc-link-voltage characteristic, it can obtain the least switching loss and switching noise and the best compensating performances, compared with the conventional fixed and newly adaptive dc-voltage-controlled LC-HAPFs. The design procedures of the dc-link voltage controller are discussed, so that the proportional and integral gains can be designed accordingly. Moreover, the general design procedures for the adaptive dc-voltage-controlled LC-HAPF with a neutral inductor are also given. The validity and effectiveness of the adaptive dc-link voltage-controlled LC-HAPF with a neutral inductor are confirmed by experimental results obtained from a 220-V 10-kVA laboratory prototype compared with the conventional fixed and adaptive dc-link voltage-controlled LC-HAPFs without a neutral inductor.**

***Index Terms*—Active power filters (APFs), current harmonics, dc-link voltage control, hybrid APFs (HAPFs), passive power filters (PPFs), reactive power.**

I. Introduction

NOWADAYS, with the proliferation and increase use of power electronics devices (nonlinear loads) and motor loadings, such as converters, adjustable speed drives, arc furnaces, bulk rectifiers, power supplies, computers, fluorescent lamps, elevators, escalators, large air conditioning systems, and compressors [1]–[10], they will mainly generate reactive power and harmonic current (third, fifth, seventh, ninth, etc.) problems into the distribution power systems. High-current harmonic distortion causes various problems in both distribution systems and consumer products, such as equipment overheating, maloperation of protection devices, and transformer overheating. The larger the reactive power, the larger the system losses and the lower the network stability. Due to these reasons, electrical utilities usually charge the industrial and commercial customers a higher electricity cost with low-power-factor situation.

Since the first installation of passive power filters (PPFs) in the mid-1940s, PPFs have been widely used to suppress current harmonics and compensate reactive power in distribution power systems due to their low cost, simplicity, and high-efficiency characteristics. Unfortunately, they have many disadvantages such as low dynamic performance, resonance problems, and filtering characteristic that is easily affected by small variations of the system parameters [1]–[5], [9], and [10]. Active power filters (APFs) can overcome the disadvantages inherent in PPFs, but their initial and operational costs are relatively high [1], [9], [10] because a high dc-link operating voltage is necessary. To provide a cost-effective solution for compensating harmonic current and reactive power problems in distribution power systems, different hybrid APF (HAPF) topologies composed of active and passive parts in series and/or parallel have been proposed in [1]–[10]. Among different HAPF topologies, a transformer-less LC coupling HAPF (LC-HAPF) has been recently proposed, applied for current quality compensation and damping of harmonic propagation [6]–[9], in which it has less passive components and low-dc-operating-voltage characteristics. To reduce cost and size of their coupling LC, they are conventionally tuned at the fifth- or seventh-order harmonic frequencies. In addition, the existing LC-HAPFs [6]–[9] are all operating at a fixed dc-link voltage level and cannot perform dynamic reactive power compensation.

To reduce the switching loss and switching noise without adding-in the soft-switching circuit and implement the dynamic reactive power compensation capability, the authors in [11] have proposed an adaptive dc-link voltage-controlled LC-HAPF for reactive power compensation. However, the proposed adaptive dc control algorithm did not include current harmonic consideration. When the loading third-order harmonic current exists significantly, the LC-HAPF filtering performances can be improved by adding a small tuned coupling neutral inductor or capacitor [12], [13]. However, the proposed LC-HAPF with

Manuscript received December 5, 2012; revised March 19, 2013 and May 24, 2013; accepted July 9, 2013. Date of publication August 1, 2013; date of current version December 20, 2013. This work was supported by the Science and Technology Development Fund (Project 015/2008/A1), Macao SAR Government and Research Committee, University of Macau, Macao, China.

C.-S. Lam, M.-C. Wong, W.-H. Choi, and X.-X. Cui are with the Department of Electrical and Computer Engineering, Faculty of Science and Technology, University of Macau, Macao, China (e-mail: cslam@umac.mo; c.s.lam@ieee.org; mcwong@umac.mo; hei_choi@ieee.org; sunstarcxx@msn.com).

H.-M. Mei and J.-Z. Liu are with the Department of Electrical Engineering, Tsinghua University, Beijing, China (e-mail: bloeim@gmail.com; liujianzheng@263.net).

Color versions of one or more of the figures in this paper are available online at http://ieeexplore.ieee.org.

Digital Object Identifier 10.1109/TIE.2013.2276037

a neutral inductor [12], [13] is operating at a fixed dc-link voltage, and its adaptive dc voltage control algorithm is still absent. Furthermore, the important proportional and integral (PI)-gain design procedures for the dc-link voltage controller including stability study and dynamic performance analysis are not being considered and analyzed in [11]–[13]. Due to the limitations among the exiting literatures, this paper aims the following:

1) to propose an adaptive dc-link voltage-controlled LC-HAPF with a neutral inductor for both dynamic reactive power and current harmonic compensation, so that the switching loss, switching noise, and compensating performances can be reduced and improved, compared with the existing LC-HAPFs;
2) to introduce the design procedures for a novel dc-link voltage controller including the stability study and dynamic performance analysis;
3) to present the general design procedures for the proposed adaptive dc controlled LC-HAPF with a neutral inductor.

As this paper mainly focuses on the aforementioned three aspects of the LC-HAPF, the consideration of unbalanced current compensation is not covered in this paper.

In the following, three-phase four-wire center-split LC-HAPFs without and with a coupling neutral inductor will be presented and compared. Then, the design criteria of its system parameters are given in Section II. Based on its single-phase equivalent circuit models in the *a–b–c* coordinates, the required minimum dc-link voltages without and with a neutral inductor can be obtained. The main contribution of this paper on the adaptive dc-link voltage controller for the LC-HAPF in both reactive power and current harmonic compensation is described in Section III. Finally, a 220-V 10-kVA LC-HAPF laboratory prototype is constructed and tested; representative experimental results are given in Section IV. Given that most of the loads in the distribution power systems are inductive, the following analysis and discussion will only focus on inductive loads [14].

II. Design of Three-Phase Four-Wire LC-HAPFs Without and With L_N

Three-phase four-wire center-split LC-HAPFs without and with a coupling neutral inductor L_n are shown in Fig. 1, where the subscript "x" denotes phase a, b, c, n. v_{sx} is the system voltage, v_x is the load voltage, and L_s is the system inductance normally neglected due to its low value relatively; thus, $v_{sx} \approx v_x$. i_{sx}, i_{Lx}, and i_{cx} are the system, load, and inverter currents for each phase, respectively. C_c and L_c are the coupling capacitor and inductor, respectively. $C_{\rm dc}$, $V_{{\rm dc}U}$, and $V_{{\rm dc}L}$ are the dc capacitor upper, and lower dc capacitor voltages with $V_{{\rm dc}U} = V_{{\rm dc}L} = 0.5V_{\rm dc}$. The load is a nonlinear load, a linear load, or their combination. In practical, due to wide usage of personal computers, uninterruptible power supplies, and various office and consumer electronic devices in residential, commercial, and office buildings, the dominant current harmonics are usually $6k \pm 1$th and $3k$th harmonics, and the even harmonics are almost zero; thus, the following analysis will be focused on $6k \pm 1$th and $3k$th harmonic orders only.

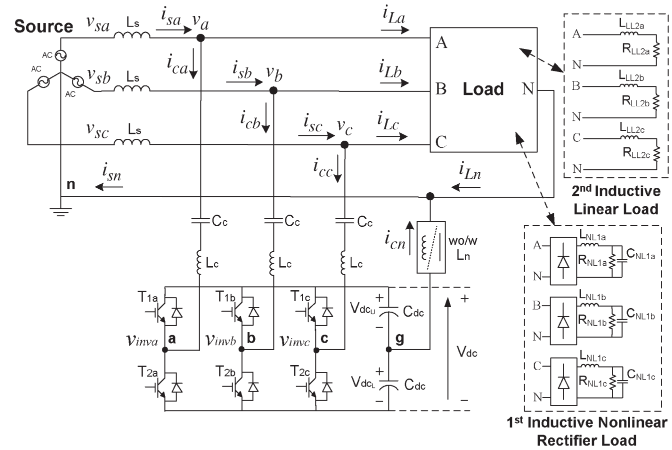

Fig. 1. Three-phase four-wire center-split LC-HAPFs without and with L_n.

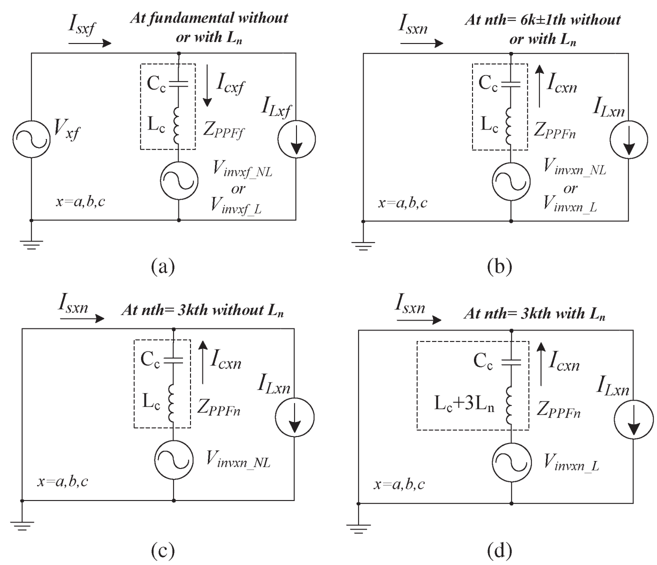

Fig. 2. LC-HAPF single-phase equivalent circuit models in the *a–b–c* coordinates. (a) At fundamental frequency without or with L_n. (b) At $nth = 6k \pm 1$th harmonic order frequency without or with L_n. (c) At $nth = 3k$th harmonic order frequency without L_n. (d) At $nth = 3k$th harmonic order frequency with L_n.

From [13], the LC-HAPF with L_n can achieve two different resonant frequencies ($3k$th and $6k \pm 1$th, $6k \pm 1$th $> 3k$th) for harmonic current filtering, while the LC-HAPF without L_n case only has one ($6k \pm 1$th or $3k$th). Fig. 2 shows its single-phase equivalent circuit models in the *a–b–c* coordinates, where the subscripts "f" and "n" denote the fundamental and harmonic frequency components, respectively, and "_NL" and "_L" denote the systems without and with L_n, respectively. Fig. 2 can help to determine the minimum dc-link operating voltage of LC-HAPF.

A. Design of Coupling C_c, L_c, and Neutral L_n

The coupling C_c and L_c are designed based on the average fundamental reactive power consumption and an $n_1 = 6k \pm 1$th dominant harmonic current order of the loading

$k = 1, 2, \ldots, \infty$. The reactance of the coupling C_c and L_c can be expressed as

$$X_{Cc} = \frac{V_x^2}{\left|\overline{Q}_{Lx_f}\right|} + X_{Lc} \qquad X_{Lc} = \frac{1}{n_1^2} X_{Cc} \tag{1}$$

where V_x is the root mean square (rms) load voltage and $\overline{Q}_{Lx_f}$ is the phase average fundamental reactive power consumption of the loading. From (1), C_c can be found

$$C_c = \left(\frac{n_1^2 - 1}{n_1^2}\right) \frac{\left|\overline{Q}_{Lx_f}\right|}{2\pi f \cdot V_x^2}. \tag{2}$$

Then, the coupling L_c can be expressed as

$$L_c = \frac{1}{(n_1 \cdot 2\pi f)^2 \cdot C_c} \tag{3}$$

where L_c can also smooth the inverter output current ripple. Moreover, the coupling neutral inductor L_n can be obtained as

$$L_n = \frac{1}{3}\left(\frac{1}{(n_2 \cdot 2\pi f)^2 \cdot C_c} - L_c\right) \tag{4}$$

where n_2 is a $3k$th harmonic current order, and $n_1 > n_2$.

B. Design of Minimum DC-Link Voltage

The switching loss of the switching device can be classified as turn-on and turnoff losses. Equation (5) is the total turn-on and turnoff power loss [15], where V_{dc}, I_{CM}, I_{CN}, t_{rN}, t_{fN}, and f_{sw} are the dc-link voltage, maximum collector current, rated collector current, rated rise time, rated fall time, and switching frequency, respectively. Thus, the higher the dc-link voltage of the LC-HAPF, the higher the switching loss obtained and vice versa

$$P_{\mathrm{Loss}} = V_{\mathrm{dc}} I_{CM} f_{\mathrm{sw}} \left(\frac{1}{8} t_{rN} \frac{I_{CM}}{I_{CN}} + t_{fN}\left(\frac{1}{3\pi} + \frac{1}{24}\frac{1_{CM}}{1_{CN}}\right)\right). \tag{5}$$

In addition, the current tracking speed of the LC-HAPF is directly proportional to the voltage difference between its dc-link voltage and load voltage, and inversely proportional to its LC impedance. For each reference compensating current, there is an optimum dc voltage to get balance between the performances and suppressing switching noise [16]. If the minimum dc-link voltage is found, it can optimize the LC-HAPF performances, switching loss, and switching noise.

From Fig. 2, [11], and [13], the required minimum dc-link voltage for compensating the reactive power ($V_{\mathrm{dc}xf\_NL}$ and $V_{\mathrm{dc}xf\_L}$) and each nth current harmonic order ($V_{\mathrm{dc}xn\_NL}$ and $V_{\mathrm{dc}xn\_L}$) can be calculated by (6)–(8) in Table I. Then, the minimum dc-link voltage requirements ($V_{\mathrm{dc}x\_NL}$ and $V_{\mathrm{dc}x\_L}$) for the single-phase equivalent circuit models can be obtained by (10) and (12) in Table I. From (7) and (8) in Table I, when L_n is added, the LC-HAPF does not require voltage for compensating the dominant $n_2 = 3k$th harmonic current, thus reducing its minimum dc-link voltage.

As the minimum dc-link voltage is calculated based on the single-phase circuit as in Fig. 2, the single-phase pq theory [17]

TABLE I
MINIMUM DC-LINK VOLTAGE DEDUCTION STEPS OF THE THREE-PHASE FOUR-WIRE LC-HAPFS WITHOUT AND WITH L_N [11], [13]

1) Fundamental Frequency	Minimum dc-link voltage without and with L_n for compensating reactive power: $V_{dcxf\_NL} = V_{dcxf\_L} = \sqrt{2}\, V_{invxf\_NL} = \sqrt{2}\, V_{invxf\_L} = \sqrt{2}\, V_x \left\| 1 - \frac{Q_{Lxf}}{\|Q_{cxf\_PPF}\|} \right\|$ where Q_{Lxf} is loading fundamental reactive power, Q_{cxf_PPF} is the reactive power provided by coupling LC.	(6)
2) Harmonic Frequencies	Minimum dc-link voltage without and with L_n for compensating each *nth* order current harmonic: $V_{dcxn\_NL} = \sqrt{2}V_{invxn\_NL} = \sqrt{2}\left\| n\omega L_c - \frac{1}{n\omega C_c} \right\| \|I_{cxn}\|$	(7)
	$V_{dcxn\_L} = \sqrt{2}V_{invxn\_L} = \begin{cases} \sqrt{2}V_{invx6k\pm1\_L} = \sqrt{2}\left\|(6k\pm1)\omega L_c - \frac{1}{(6k\pm1)\omega C_c}\right\| \|I_{cx6k\pm1}\| \\ \sqrt{2}V_{invx3k\_L} = \sqrt{2}\left\|3k\omega(L_c+3L_n) - \frac{1}{3k\omega C_c}\right\| \|I_{cx3k}\| \end{cases}$ where $\|I_{cxn}\|=\|I_{Lxn}\|$, $nth=6k\pm1th$ or $3kth$, $k=1, 2\ldots\infty$, $n=2, 3\ldots\infty$, $\omega=2\pi f$	(8)
3) All Frequencies	Minimum dc-link voltage without and with L_n: $V_{dc\_NL} = V_{dc\_min} = \max(2V_{dca\_NL}, 2V_{dcb\_NL}, 2V_{dcc\_NL})$	(9)
	Where $V_{dcx\_NL} = \sqrt{\left\|V_{dcxf\_NL}\right\|^2 + \sum_{n=2}^{\infty}\left\|V_{dcxn\_NL}\right\|^2}$	(10)
	$V_{dc\_L} = V_{dc\_min} = \max(2V_{dca\_L}, 2V_{dcb\_L}, 2V_{dcc\_L})$	(11)
	Where $V_{dcx\_L} = \sqrt{\left\|V_{dcxf\_L}\right\|^2 + \sum_{n=2}^{\infty}\left\|V_{dcxn\_L}\right\|^2}$ where $n=2, 3\ldots\infty$	(12)

is being chosen; thus, the reactive power and current harmonics in each phase can be compensated independently, and the final minimum dc-link voltages for the three-phase four-wire LC-HAPFs without and with L_n (V_{dc_NL} and V_{dc_L}) will be the maximum ones among the calculated minimum values of each phase indicated by (9) and (11) in Table I. Therefore, the calculated dc-link voltage must be sufficient for all three phases. In the next section, the adaptive dc-link voltage controller for the three-phase four-wire LC-HAPFs without and with L_n will be proposed. Moreover, the controller also works for the LC-HAPF initial start-up dc-link self-charging function.

III. PROPOSED ADAPTIVE DC-LINK VOLTAGE CONTROLLER FOR LC-$HAPFs$ WITHOUT AND WITH L_N

Fig. 3 shows the proposed adaptive dc-link voltage control block diagram for the three-phase four-wire LC-HAPFs without and with L_n, in which it consists of three main control blocks: instantaneous power compensation control block, proposed adaptive dc-link voltage control block, and final reference compensating current and pulsewidth-modulation (PWM) control block.

A. Instantaneous Power Compensation Control Block

For the instantaneous power compensation control block, the reference reactive and harmonic compensating currents for

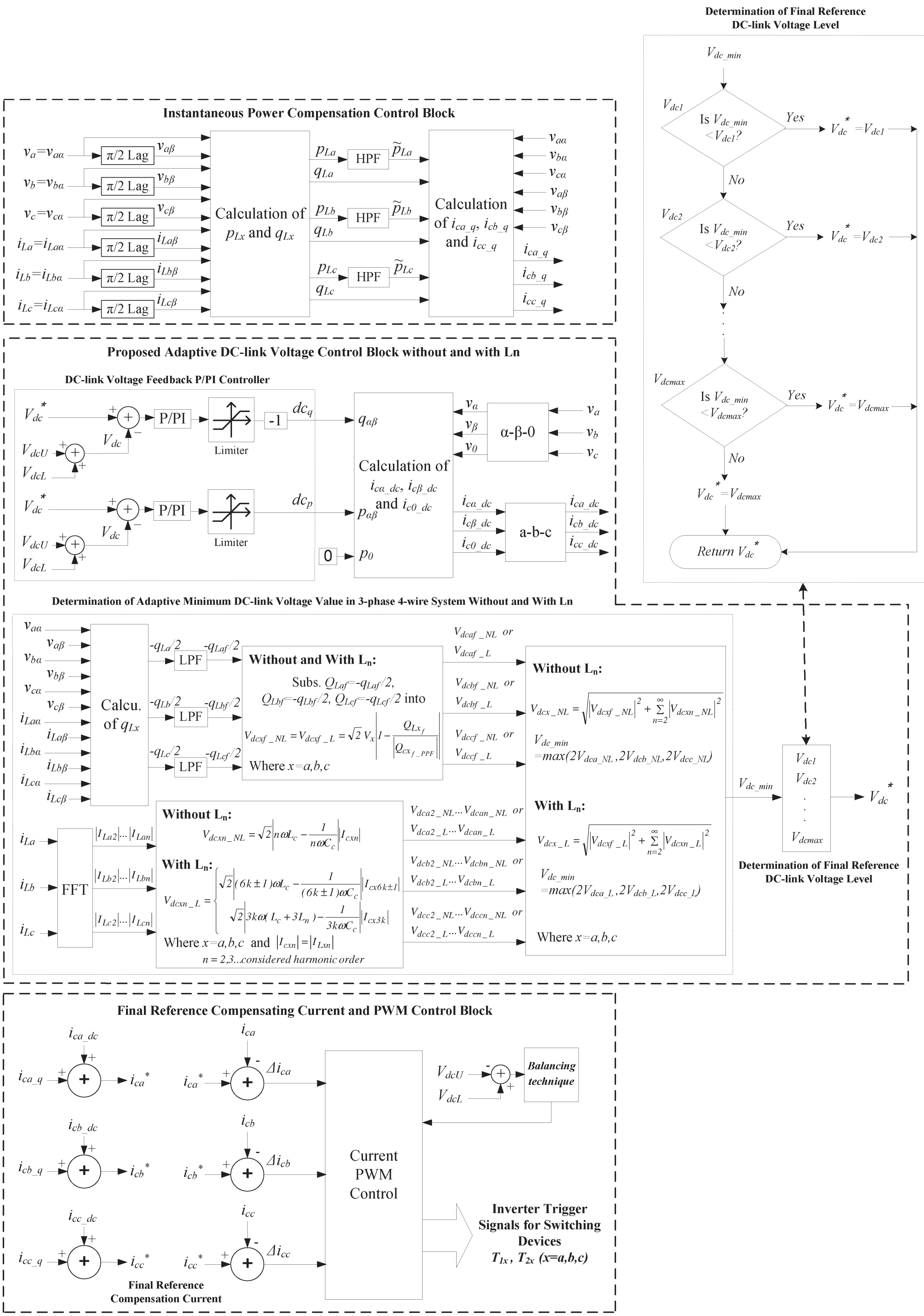

Fig. 3. Proposed adaptive dc-link voltage control block diagram for the three-phase four-wire LC-HAPFs without and with L_n.

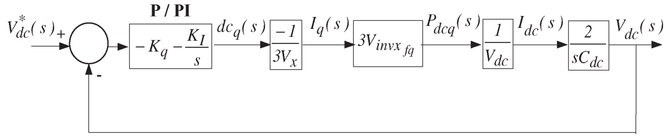

Fig. 4. Block diagram of dc-link voltage control during adaptive dc voltage control and start-up dc-link self-charging function.

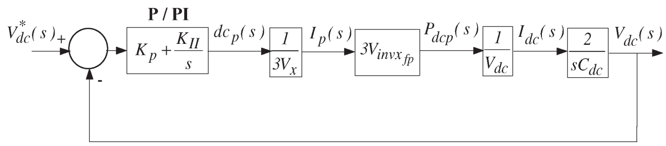

Fig. 5. Block diagram of dc-link voltage control during compensating system loss.

LC-HAPF (i_{cx_q}, the subscript $x = a, b, c$ for three phases) are determined by the single-phase instantaneous pq theory [17].

B. Proposed Adaptive DC-Link Voltage Control Block

The adaptive dc-link voltage control block consists of three parts: 1) determination of adaptive minimum dc-link voltage $V_{\mathrm{dc\_min}}$; 2) determination of final reference dc-link voltage level V_{dc}^*; and 3) dc-link voltage feedback P/PI controller.

1) Determination of Adaptive Minimum DC-Link Voltage: The loading instantaneous fundamental reactive power in each phase q_{Lxf} is calculated by using the single-phase instantaneous pq theory [17] and low-pass filters. Usually, $-q_{Lxf}/2$ can keep a constant value for more than one cycle; thus, the loading fundamental reactive power consumption Q_{Lxf} in each phase can be approximately treated as $Q_{Lxf} \approx -q_{Lxf}/2$. Then, the required minimum dc-link voltage for compensating each phase Q_{Lxf} can be calculated by using (6) in Table I. With the help of fast Fourier transform, the load current spectra $|I_{Lxn}|$ up to the considered current harmonic order n can be calculated; the required minimum dc-link voltage for compensating each nth order current harmonic can be calculated by using (7) and (8) in Table I. With the help of (10) and (12) in Table I, the adaptive minimum dc-link voltages $V_{\mathrm{dc\_min}}$ for the three-phase four-wire LC-HAPFs without and with L_n can be determined by (9) and (11) in Table I accordingly. To implement the adaptive dc voltage control function for the LC-HAPF, $V_{\mathrm{dc\_min}}$ can be simply treated as the final reference dc voltage V_{dc}^*. It is obvious that, when the loading is changing, the system adaptively yields different $V_{\mathrm{dc\_min}}$ values.

2) Determination of Final Reference DC-Link Voltage Level: However, this adaptive control scheme may frequently change the dc voltage reference V_{dc}^* in practical situation, as the loading is randomly determined by electric users (different Q_{Lxf} and I_{Lxn} values). Then, this frequent change would cause a rapid dc voltage fluctuation, resulting in deterioration of the LC-HAPF operating performances [18]. To alleviate this problem, a final reference dc-link voltage level determination process proposed in [11] is added, so that V_{dc}^* can be maintained as a constant value within a specific compensation range. If $V_{\mathrm{dc\_min}}$ is greater than the maximum level $V_{\mathrm{dc\,max}}$, $V_{\mathrm{dc}}^* = V_{\mathrm{dc\,max}}$.

3) DC-Link Voltage Feedback P/PI Controller: The LC-HAPF can effectively control the adaptive dc-link voltage level

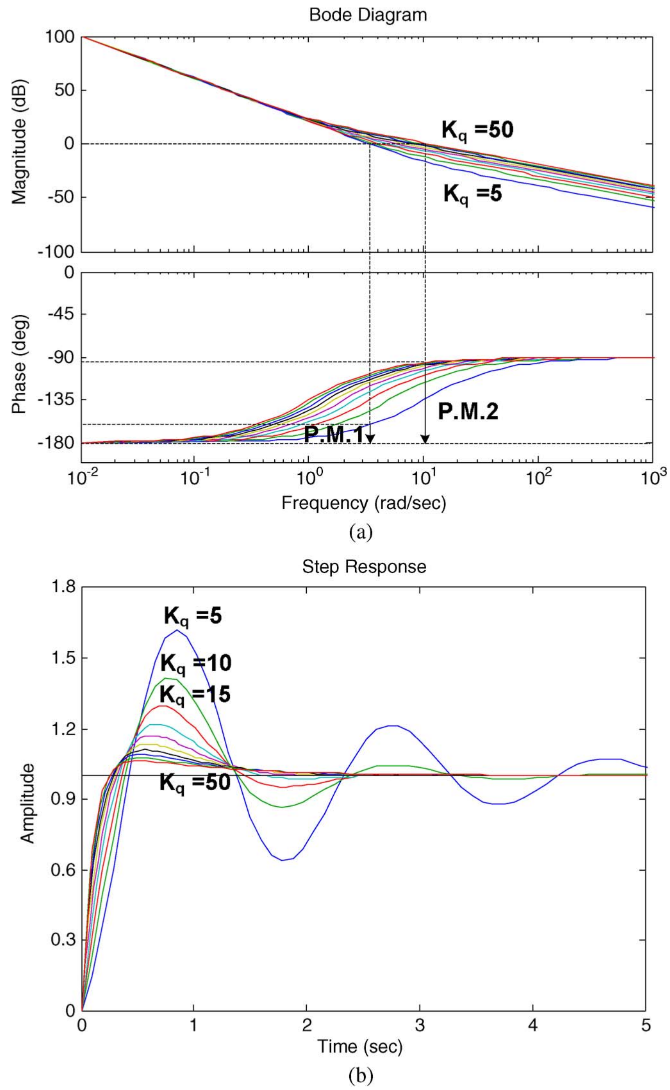

Fig. 6. Stability and dynamic response of dc voltage controller in Fig. 4 when $K_I = 50$ and K_q varies from 5 to 50. (a) Bode diagram. (b) Step response.

by feeding back the dc-voltage-controlled signal as both reactive and active current reference components (d_{cq} and d_{cp}) [19]

$$\mathrm{dc}_q = -K_q \cdot (V_{\mathrm{dc}}^* - V_{\mathrm{dc}}) - K_I \int (V_{\mathrm{dc}}^* - V_{\mathrm{dc}})\, dt \qquad (13)$$

$$\mathrm{dc}_p = K_p \cdot (V_{\mathrm{dc}}^* - V_{\mathrm{dc}}) + K_{II} \int (V_{\mathrm{dc}}^* - V_{\mathrm{dc}})\, dt \qquad (14)$$

where dc_q aims to change the dc-link voltage level due to adaptive dc control and start-up dc-link self-charging function, while dc_p aims to maintain the dc-link voltage due to the system loss. K_q and K_p are the proportional gains, while K_I and K_{II} are the integral gains of the controllers. With the help of the three-phase instantaneous pq theory [20] and the dc_q and dc_p terms, the dc-link voltage V_{dc} can track its reference V_{dc}^* by changing the three-phase dc voltage control reference compensating currents i_{cx_dc} in the a–b–c coordinates, in which the calculation details are discussed in [19]. In the following, the design process for K_q, K_p, K_I, and K_{II} will be discussed.

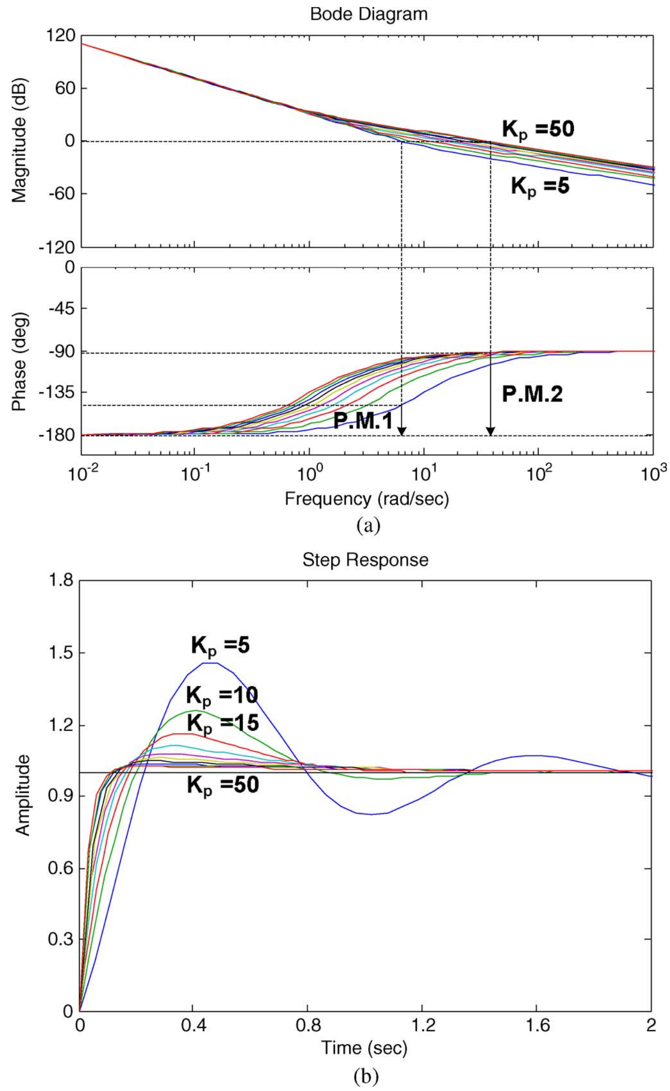

Fig. 7. Stability and dynamic response of dc voltage controller in Fig. 5 when $K_{II} = 50$ and K_p varies from 5 to 50. (a) Bode diagram. (b) Step response.

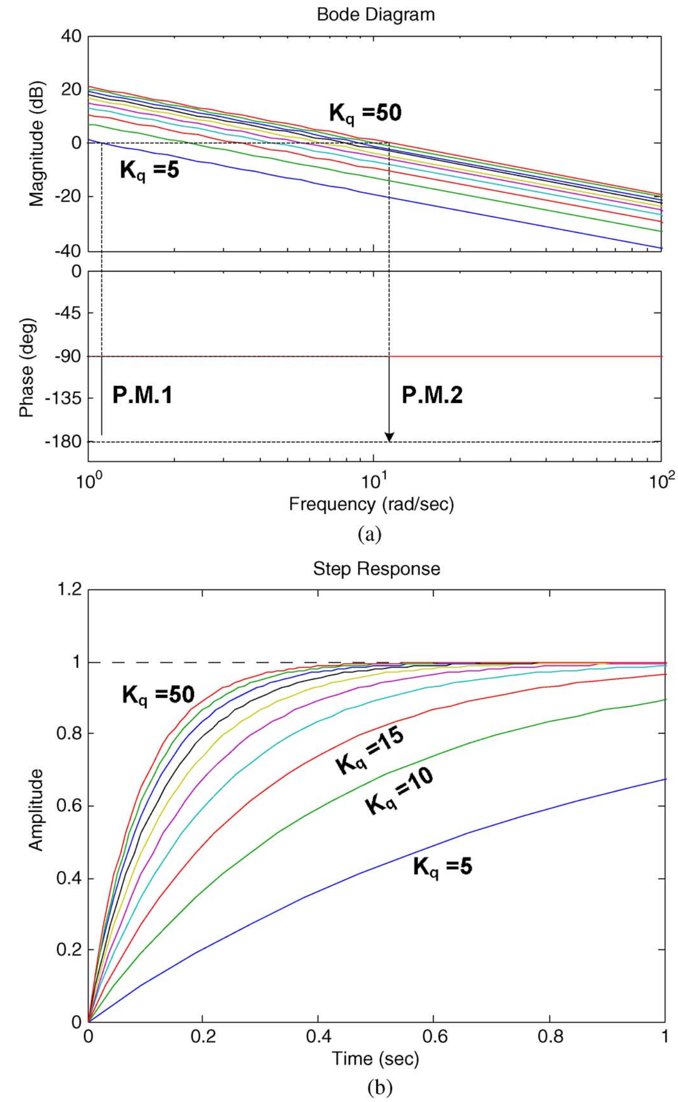

Fig. 8. Stability and dynamic response of dc-link voltage controller in Fig. 4 when K_q varies from 5 to 50. (a) Bode diagram. (b) Step response.

Fig. 4 shows the dc-link voltage control block diagram during adaptive dc control and start-up dc-link self-charging function, and Fig. 5 shows the dc-link voltage control block diagram during compensating system loss, where $V_{\mathrm{inv}xfp} = |V_x - |I_{cxfq}| X_{PPFf}\|$ and $V_{\mathrm{inv}xfq} = |I_{cxfp}\| X_{PPFf}|$ are the inverter fundamental active and reactive voltages, respectively, and I_{cxfp} and I_{cxfq} are the fundamental compensating active and reactive currents, respectively.

When PI controller is applied, from Figs. 4 and 5, their close-loop transfer functions can be expressed as

$$\frac{V_{\mathrm{dc}}(s)}{V_{\mathrm{dc}}^*(s)} = \frac{\frac{2V_{\mathrm{inv}xfq}K_q}{V_x V_{\mathrm{dc}} C_{\mathrm{dc}}} s + \frac{2V_{\mathrm{inv}xfq}K_I}{V_x V_{\mathrm{dc}} C_{\mathrm{dc}}}}{s^2 + \frac{2V_{\mathrm{inv}xfq}K_q}{V_x V_{\mathrm{dc}} C_{\mathrm{dc}}} s + \frac{2V_{\mathrm{inv}xfq}K_I}{V_x V_{\mathrm{dc}} C_{\mathrm{dc}}}} \quad \text{(Fig. 4)} \tag{15}$$

$$\frac{V_{\mathrm{dc}}(s)}{V_{\mathrm{dc}}^*(s)} = \frac{\frac{2V_{\mathrm{inv}xfp}K_p}{V_x V_{\mathrm{dc}} C_{\mathrm{dc}}} s + \frac{2V_{\mathrm{inv}xfp}K_{II}}{V_x V_{\mathrm{dc}} C_{\mathrm{dc}}}}{s^2 + \frac{2V_{\mathrm{inv}xfp}K_p}{V_x V_{\mathrm{dc}} C_{\mathrm{dc}}} s + \frac{2V_{\mathrm{inv}xfp}K_{II}}{V_x V_{\mathrm{dc}} C_{\mathrm{dc}}}} \quad \text{(Fig. 5).} \tag{16}$$

By the Routh–Hurwitz criterion, the Routh tables for (15) and (16) can be obtained. As K_q, K_p, K_I, and $K_{II} > 0$, the dc voltage controllers will be stable. From the LC-HAPF experimental system parameters in Table IV, $C_c = 50\ \mu$F, $L_c = 8$ mH, $C_{\mathrm{dc}} = 3.3$ mF, and $V_x = 220$ V. For the dc-link maximum operating voltage is $V_{\mathrm{dc}} = 150$ V, the fundamental compensating active and reactive currents are $|I_{cxfp}| = 0.2$ A and $|I_{cxfq}| = 4.2$ A, when $K_I = K_{II} = 50$, the effects of K_q and K_p to the controller's stability and dynamic response are shown in Figs. 6 and 7. From Figs. 6 and 7, when K_q and K_p are varying from 5 to 50, their phase margins are increasing from P.M.1 to P.M.2, which enhances the controllers' stability. Moreover, larger K_q and K_p values will yield a faster dynamic response for the controllers.

When only P controller is applied, i.e., $K_I = K_{II} = 0$ in Figs. 4 and 5, their close-loop transfer functions can be deduced from (15) and (16). By the Routh tables, as K_q and $K_p > 0$, the dc voltage controllers will be stable. If the proportional gains K_q and K_p are set too large, they produce a large fluctuation during steady state. On the contrary, if they are set too small, a long settling time and a large steady-state error will occur. In addition, the effects of K_q and K_p to the controllers' stability and dynamic response are shown in Figs. 8 and 9. From Figs. 8 and 9, when K_q and K_p are varying from 5 to 50, their

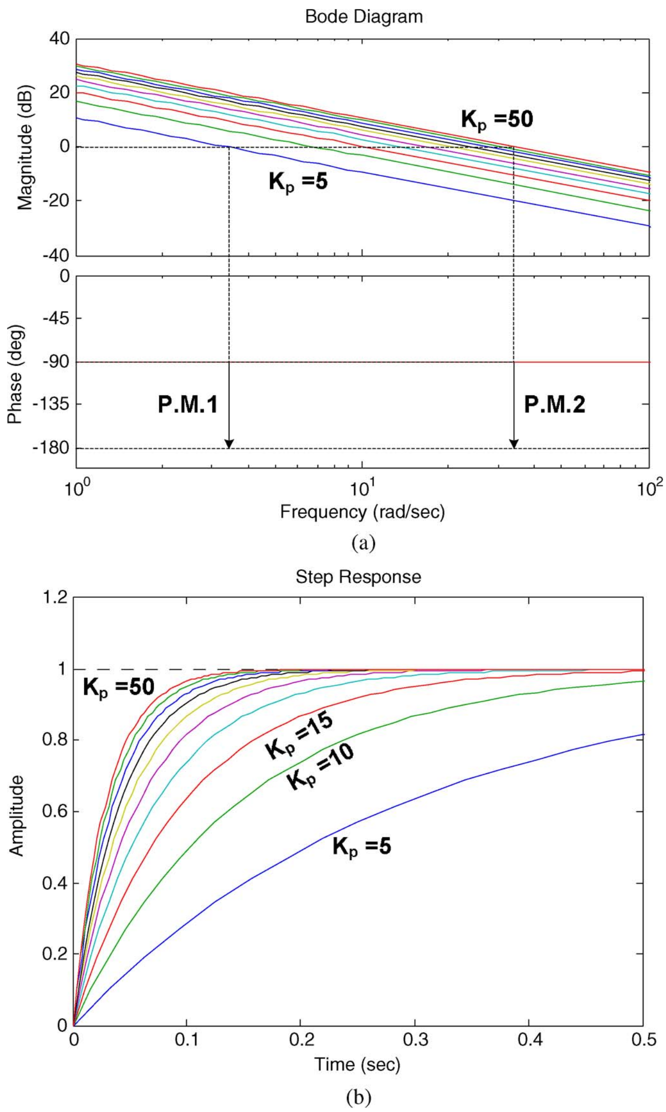

Fig. 9. Stability and response dynamic of dc-link voltage controller in Fig. 5 when K_P varies from 5 to 50. (a) Bode diagram. (b) Step response.

phase margins (P.M.1 and P.M.2) do not change at all, and the controllers obtain good stability. Moreover, larger K_q and K_p values will yield a faster dynamic response.

To simplify the control process, dc_q and dc_p in (13) and (14) can be calculated by the same controller, i.e., $K_q = K_p$, and $K_I = K_{II}$. Even though the P controller yields a steady-state error, it is chosen in this paper because of its simplicity and memory resource saving in the digital signal processor (DSP); therefore, it can yield a faster response than the PI controller, as verified by Figs. 6(b)–9(b). Moreover, $K_q = K_p = 40$ is selected in this paper. If the dc-link voltage with zero steady-state error is taken in consideration, the PI controller is appreciated, and $K_q = K_p = 40$ and $K_I = K_{II} = 50$ can be chosen. A limiter is also applied to avoid the overflow problem of the controllers.

C. Final Reference Compensating Current and PWM Control Block

Both hysteresis PWM and triangular carrier-based sinusoidal PWM methods can be applied for the PWM control part. After

TABLE II
EXPERIMENTAL PARAMETERS FOR TESTING LOADING

System Parameters			Physical Values
V_x, f			220V$_{\mathrm{rms}}$, 50Hz
1st inductive nonlinear rectifier load	A, B, C	R_{NL1x}, L_{NL1x}, C_{NL1x}	43.2Ω, 34.5mH, 392.0μF ($Q_{Lxf} \approx$ 720.0var)
2nd inductive linear load	A, B, C	R_{LL2x}, L_{LL2x}	60Ω, 70mH ($Q_{Lxf} \approx$ 200.0var)

TABLE III
EXPERIMENTAL THIRD-, FIFTH-, SEVENTH-, AND NINTH-ORDER HARMONIC CURRENT VALUES

Different Situations:		Harmonic Current Order			
		3rd	5th	7th	9th
1st loading	A,B,C	1.92A	0.45A	0.20A	0.12A
1st & 2nd loadings	A,B,C	1.90A	0.46A	0.23A	0.12A

TABLE IV
SYSTEM PARAMETERS FOR THE 220-V 10-kVA THREE-PHASE FOUR-WIRE LC-HAPF

System Parameters		Physical Values
Passive part	L_c, C_c, L_n	8mH, 50uF, 5mH
DC capacitor	C_{dc}	3.3mF
DC-link voltage levels	V_{dcU} , V_{dcL}	25V, 50V, 75V

TABLE V
LC-HAPF EXPERIMENTAL MINIMUM DC-LINK VOLTAGE LEVELS

Different Situations:			Required $V_{dc\_min}/2$	Final Minimum Adapt. Level V_{dcU},V_{dcL}
L_n=0mH	1st loading	A,B,C	44.0V	50V
	1st & 2nd loadings	A,B,C	58.3V	75V
L_n=5mH	1st loading	A,B,C	25.3V	25V
	1st & 2nd loadings	A,B,C	46.3V	50V

the process of instantaneous power compensation and adaptive dc voltage control blocks, as shown in Fig. 3, the final reference compensating current i^*_{cx} can be obtained by summing up the i_{cx_q} and i_{cx_dc}. Then, the final reference and actual compensating currents i^*_{cx} and i_{cx} will be sent to the PWM control part, and the PWM trigger signals for the switching devices can then be generated. If the three-phase loadings are unbalanced, dc capacitor voltage imbalance may occur; the dc capacitor voltage balancing concepts and techniques in [21] can be applied to balance the $V_{\mathrm{dc}U}$ and $V_{\mathrm{dc}L}$ under the adaptive dc voltage control method.

D. General Design Procedures for Adaptive DC-Link Voltage-Controlled LC-HAPF With L_n

The general design procedures for the adaptive dc-link voltage-controlled LC-HAPF with L_n, as shown in Fig. 1, will be summarized in the following steps.

1) From the average $\overline{Q}_{Lxf}$, dominant $n_1 = 6k \pm 1$th and $n_2 = 3k$th, $n_1 > n_2$, C_c, L_c, and L_n can be designed by (1)–(4).
2) V_{dcmax} is designed according to the specification of LC-HAPF; $V_{\mathrm{dcmax}}/3$ or $V_{\mathrm{dcmax}}/4$ can be treated as each dc voltage level step size.

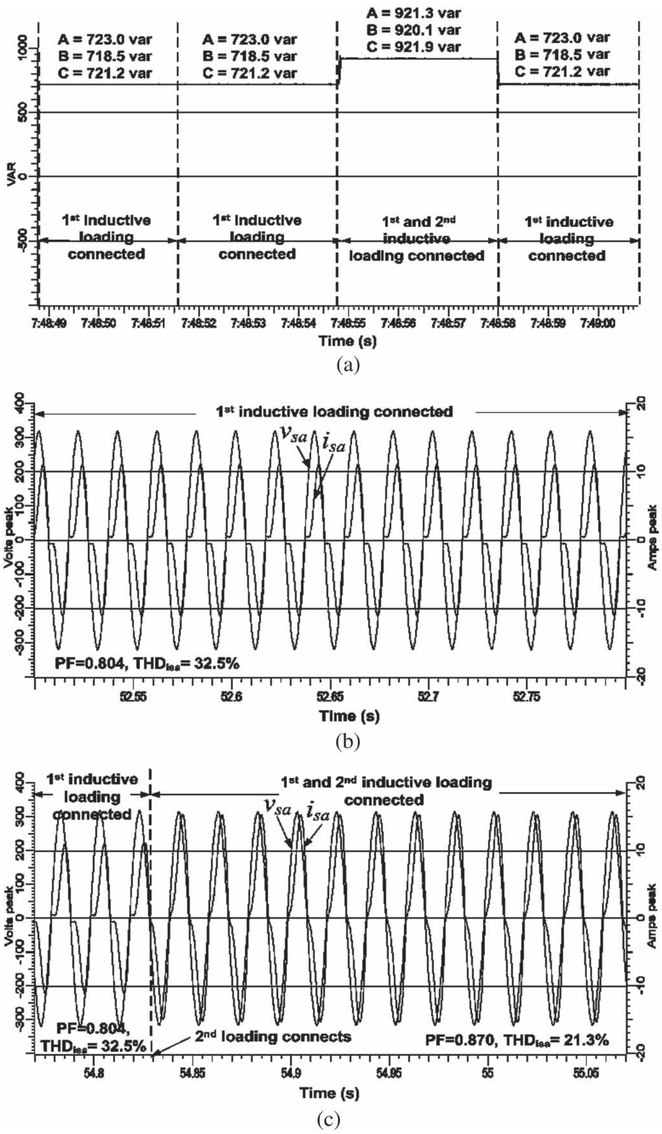

Fig. 10. Before LC-HAPF compensation. (a) Q_{sxf}. (b) v_x and i_{sx} of phase a when the first loading is connected. (c) v_x and i_{sx} of phase a when the first and second loadings are connected.

TABLE VI
EXPERIMENTAL RESULTS BEFORE LC-HAPF COMPENSATION

Before LC-HAPF Compensation for Testing Loading							
Different Cases:		Q_{sxf} (var)	PF	THD_{isx} (%)	THD_{vx} (%)	i_{sx} (A_{rms})	i_{sn} (A_{rms})
1st inductive loading	A	723.0	0.804	32.5	1.7	6.506	5.808
	B	718.5	0.805	31.5	1.9	6.467	
	C	721.2	0.804	31.6	1.5	6.444	
1st and 2nd inductive loading	A	921.3	0.870	21.3	1.6	9.520	5.659
	B	920.1	0.872	20.5	1.8	9.539	
	C	921.9	0.870	20.7	1.5	9.493	

3) PI gains of dc voltage controller can be designed by plotting bode and step response plots of (15) and (16).
4) According to Fig. 3, the proposed adaptive dc-link voltage controller for the LC-HAPF with L_n can be implemented by using a DSP.
5) Sampling frequency, switching frequency, and hysteresis band of the LC-HAPF can be designed by referring to [22].

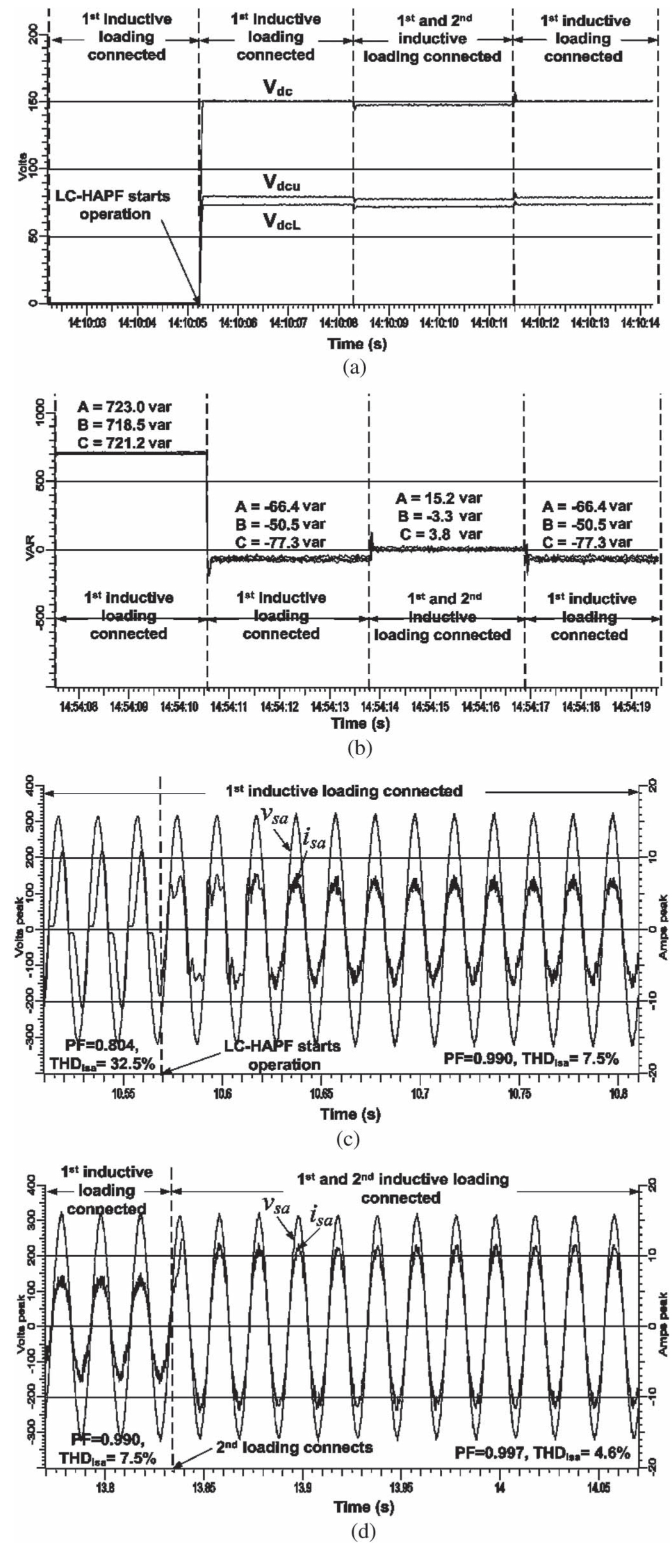

Fig. 11. LC-HAPF whole experimental dynamic compensation process with conventional fixed dc-link voltage control scheme. (a) V_{dcU} and V_{dcL}. (b) Q_{sxf}. (c) v_x and i_{sx} of phase a after LC-HAPF starts operation. (d) v_x and i_{sx} of phase a after the second loading is connected.

In the following, the adaptive dc-link voltage-controlled LC-HAPFs without and with L_n experimental compensation results will be given, compared with the conventional fixed dc-voltage-controlled LC-HAPF without L_n.

TABLE VII
EXPERIMENTAL RESULTS AFTER LC-HAPF COMPENSATION WITH FIXED DC-LINK VOLTAGE CONTROL

After LC-HAPF Compensation with Fixed DC-link Voltage Control								
Different Cases:		Q_{sxf} (var)	PF	THD_{isx} (%)	THD_{vx} (%)	i_{sx} (A_{rms})	i_{sn} (A_{rms})	V_{dcU}, V_{dcL}
1st inductive loading	A	-66.4	0.990	7.5	1.3	4.943	1.347	75V
	B	-50.5	0.990	8.7	1.2	5.024		
	C	-77.3	0.989	9.0	1.1	5.108		
1st and 2nd inductive loading	A	15.2	0.997	4.6	1.1	8.071	1.324	75V
	B	-3.3	0.997	5.2	1.0	8.036		
	C	3.8	0.997	5.8	1.1	8.023		

IV. EXPERIMENTAL VERIFICATIONS OF THE PROPOSED ADAPTIVE DC-LINK VOLTAGE CONTROLLER FOR THE LC-HAPF

In this section, the proposed adaptive dc-link voltage-controlled LC-HAPFs without and with L_n for dynamic reactive power and current harmonic compensation will be verified by experiments. A 220-V 10-kVA LC-HAPF experimental prototype is designed and constructed in the laboratory. The control system is a DSP TMS320F2812, and its sampling frequency is set at 25 kHz. Hysteresis current PWM is applied for the experimental prototype with a hysteresis band of $H = 0.0625$ A, and the maximum switching frequency is 12.5 kHz, in which the hysteresis band and sampling frequency satisfy the LC-HAPF linearization requirement [22]. Moreover, the Mitsubishi insulated-gate bipolar transistor intelligent power modules PM300DSA60 are employed as the switching devices of the inverter, and their switching frequency limitation is at 20 kHz. Fig. 3 shows the adaptive dc-link voltage-controlled LC-HAPFs without and with L_n control block diagrams for experiments. For simplicity, the LC-HAPF system has been tested under approximately balanced loading situations. The structure of the loads and their parameters' values are shown in Fig. 1 and summarized in Table II.

For the full bridge rectifier loading as shown in Fig. 1, the third- and fifth-order harmonic currents will be the two dominant harmonic current contents of the loading. For designing the coupling passive part parameters based on average loading reactive power $\bar{Q}_{Lxf} = (920 \text{ var} + 660 \text{ var})/2 = 790.0$ var, $n_1 = 5$, and $n_2 = 3$, from (1)–(4), the system parameters can be designed as $C_c = 50.0$ μF, $L_c = 8.0$ mH, and $L_n = 5.0$ mH, respectively. The physical dimension of L_n is 14.5 cm × 8.5 cm × 14 cm with a current rating of 20 A, and the operating frequency is at 3–5 kHz. It has a quality factor of around 30. Moreover, a high quality factor for L_n is appreciated to improve its performance and reduce power loss.

As the experimental loading harmonic current contents beyond the ninth order are small, for simplicity, the required minimum dc-link voltage for current harmonic compensation will be calculated up to the ninth harmonic order only. Table III shows the third-, fifth-, seventh-, and ninth-order harmonic currents in rms values. Based on the loading situations in Tables II and III and the reactive power provided by the coupling passive part $Q_{cxf\_PPF} \approx -777.0$ var$(V_x = 218 \text{ V}) \sim -806.0$ var$(V_x = 222 \text{ V})$, the final reference V_{dc}^* is designed to have three adaptive dc voltage levels (V_{dcU}, $V_{dcL} = 25$, 50,

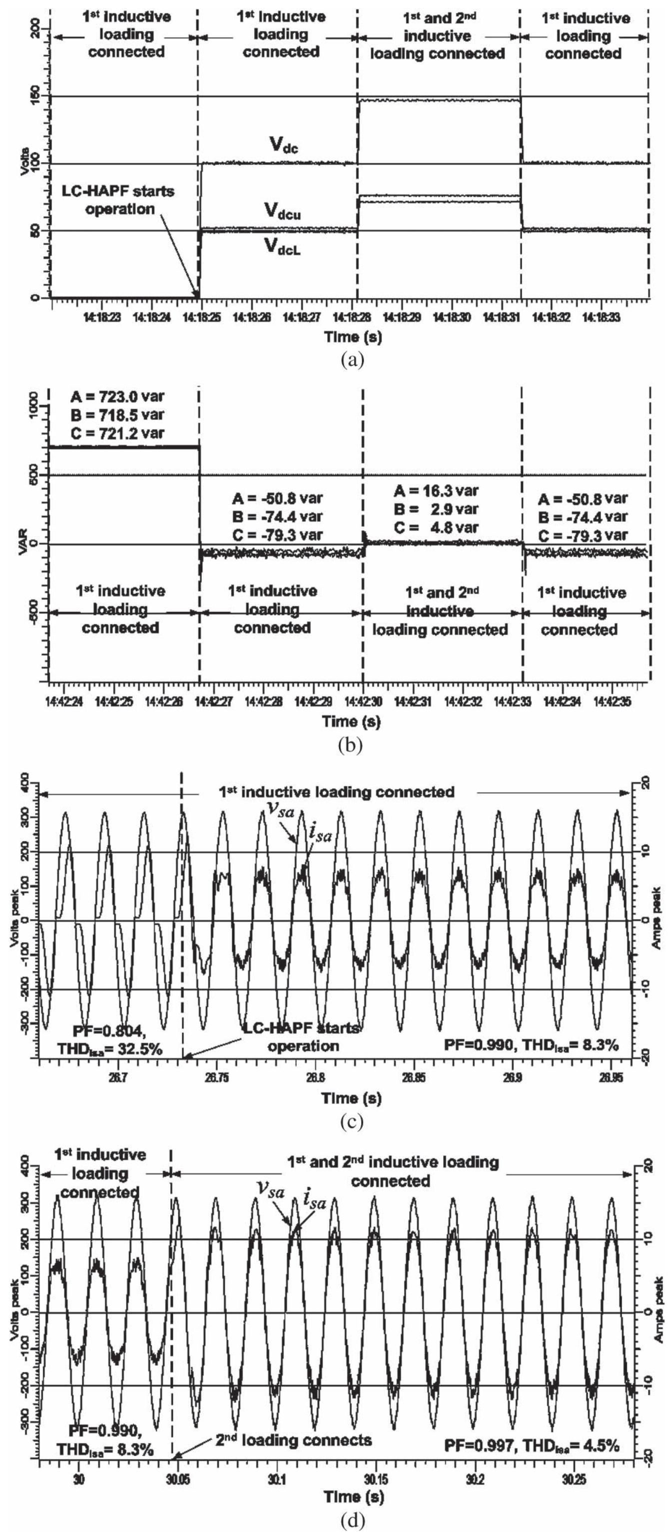

Fig. 12. LC-HAPF whole experimental dynamic compensation process with adaptive dc-link voltage control scheme. (a) V_{dcU} and V_{dcL}. (b) Q_{sxf}. (c) v_x and i_{sx} of phase a after LC-HAPF starts operation. (d) v_x and i_{sx} of phase a after the second loading is connected.

and 75 V) for the experimental verification. Table IV lists the system parameters for the 220-V 10-kVA three-phase four-wire LC-HAPF experimental prototype. From Tables I–IV, the final minimum adaptive levels V_{dcU} and V_{dcL} for the experiments are illustrated in Table V.

TABLE VIII
EXPERIMENTAL RESULTS AFTER LC-HAPF COMPENSATION WITH ADAPTIVE DC-LINK VOLTAGE CONTROL

After LC-HAPF Compensation with Adaptive DC-link Voltage Control								
Different Cases:		Q_{sxf} (var)	PF	THD_{isx} (%)	THD_{vx} (%)	i_{sx} (A_{rms})	i_{sn} (A_{rms})	V_{dcU}, V_{dcL}
1st inductive loading	A	-50.8	0.990	8.3	1.0	5.023	1.500	50V
	B	-74.4	0.989	10.3	1.1	5.044		
	C	-79.3	0.989	10.7	1.0	5.058		
1st and 2nd inductive loading	A	16.3	0.997	4.5	1.0	8.085	1.414	75V
	B	2.9	0.997	5.0	1.0	8.047		
	C	4.8	0.997	5.9	1.0	8.008		

Before the LC-HAPF performs compensation, Fig. 10 shows the experimental reactive power at system source-side Q_{sxf}, load voltage v_x, and system current i_{sx} waveforms of phase a. As the experimental loadings are approximately balanced, only v_x and i_{sx} waveforms of phase a will be illustrated. Table VI summarizes the power quality parameters for the testing loadings. When the first inductive loading is connected, the three-phase Q_{sxf} values are 723.0, 718.5, and 721.2 var with power factor $(\mathrm{PF}) = 0.804, 0.805,$ and 0.804, respectively, and the total harmonic distortion (THD_{isx}) values of i_{sx} are 32.5%, 31.5%, and 31.6%, in which the THD_{isx} does not satisfy the international standards ($\mathrm{THD}_{isx} < 16\%$ for IEC and $\mathrm{THD}_{isx} < 20\%$) [23], [24]. When both first and second inductive loadings are connected, the three-phase Q_{sxf} values increase to 921.3, 920.1, and 921.9 var with $\mathrm{PF} = 0.870, 0.872,$ and 0.870 respectively, and the THD_{isx} values become 21.3%, 20.5%, and 20.7%, in which the THD_{isx} does not satisfy the standards [23], [24]. In the following, the experimental compensation results by the following three different LC-HAPFs will be given and compared: 1) conventional fixed dc-link voltage-controlled LC-HAPF; 2) adaptive dc-link voltage-controlled LC-HAPF; and 3) adaptive dc-link voltage-controlled LC-HAPF with L_n.

With conventional fixed dc-link voltage reference ($V_{\mathrm{dc}U}$, $V_{\mathrm{dc}L} = 75$ V) for the LC-HAPF, Fig. 11(a) shows that the $V_{\mathrm{dc}U}$ and $V_{\mathrm{dc}L}$ levels can be controlled at a reference of 75 V no matter when the first loading or the first and second loadings are connected. From Fig. 11(b), the experimental Q_{sxf} can be approximately compensated close to zero for both loading cases, compared with Fig. 10(a). Fig. 11(c) shows that the PF and THD_{isx} of phase a can be improved from 0.804 to 0.990 and from 32.5% to 7.5%, respectively, at the first loading case. From Fig. 11(d), the PF and THD_{isx} of phase a become 0.997 and 4.6%, respectively, when the second loading is connected. Table VII summarizes the results of the LC-HAPF with the conventional fixed dc-link voltage control.

With the adaptive dc-link voltage control for the LC-HAPF, Fig. 12(a) shows that the $V_{\mathrm{dc}U}$ and $V_{\mathrm{dc}L}$ can be adaptively changed ($V_{\mathrm{dc}U}$, $V_{\mathrm{dc}L} = 50$ V for the first loading, and $V_{\mathrm{dc}U}$, $V_{\mathrm{dc}L} = 75$ V for the first and second loadings) according to different loading cases. From Fig. 12(b), the experimental Q_{sxf} can be compensated close to zero for both loading cases. Fig. 12(c) shows that the PF and THD_{isx} of phase a can be improved from 0.804 to 0.990 and from 32.5% to 8.3%, respectively, at the first loading case. From Fig. 12(d), the PF and THD_{isx} of phase a become 0.997 and 4.5%, respectively,

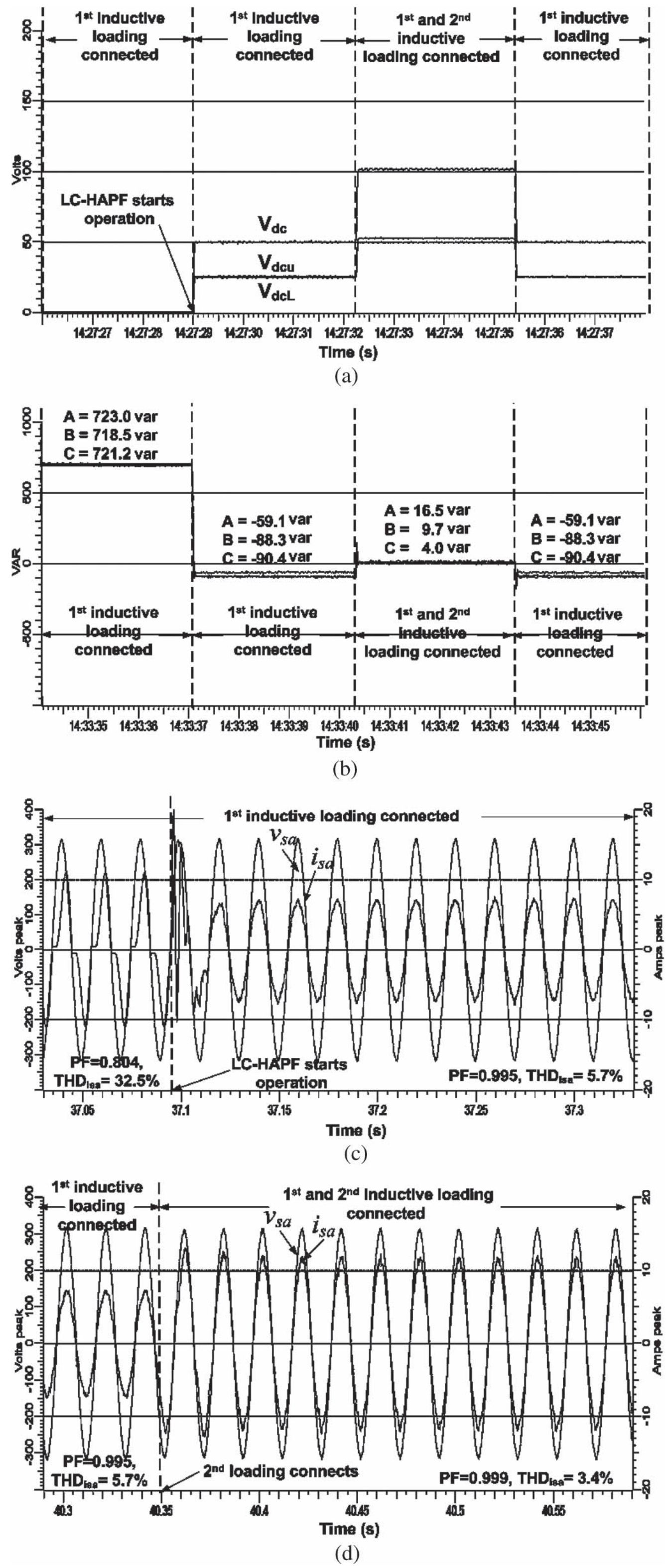

Fig. 13. LC-HAPF whole experimental dynamic compensation process with adaptive dc-link voltage control scheme and L_n. (a) $V_{\mathrm{dc}U}$ and $V_{\mathrm{dc}L}$. (b) Q_{sxf}. (c) v_x and i_{sx} of phase a after LC-HAPF starts operation. (d) v_x and i_{sx} of phase a after the second loading is connected.

when the second loading is connected. Table VIII summarizes the results of the LC-HAPF with the adaptive dc-link voltage control scheme.

With the adaptive dc-link voltage control for the LC-HAPF with L_n, Fig. 13(a) shows that the V_{dcU} and V_{dcL} can be adaptively changed (V_{dcU}, $V_{dcL} = 25$ V for the first loading, and V_{dcU}, $V_{dcL} = 50$ V for the first and second loadings) according to different loading cases. From Fig. 13(b), the experimental Q_{sxf} can be compensated close to zero for both loading cases. Fig. 13(c) shows that the PF and THD_{isx} of phase a can be improved from 0.804 to 0.995 and from 32.5% to 5.7%, respectively, at the first loading case. From Fig. 13(d), the PF and THD_{isx} of phase a become 0.999 and 3.4%, respectively, when the second loading is connected. Table IX summarizes the results of the LC-HAPF with the adaptive dc-link voltage control scheme and L_n.

From Figs. 11–13 and Tables VII–IX, the three different LC-HAPFs can achieve more or less the same steady-state reactive power compensation results, and their compensated THD_{isx} and THD_{vx} satisfy the international standards [23]–[25]. Moreover, the system current i_{sx} and neutral current i_{sn} can be significantly reduced after compensation. From Table X, during the first loading case, the adaptive dc control scheme (V_{dcU}, $V_{dcL} = 50$ V) can reduce the switching loss compared with the conventional fixed V_{dcU}, $V_{dcL} = 75$ V control, which is consistent with (5). Moreover, the adaptive dc-link voltage-controlled LC-HAPF with L_n can obtain the least switching loss because it just requires the lowest dc-link voltage levels for compensating both loading cases. The lowest dc-link voltage also leads the LC-HAPF to obtain the best current harmonics and neutral current reduction.

Fig. 14 shows the experimental compensating currents i_{cx} of phase a with (a) fixed V_{dcU}, $V_{dcL} = 75$ V, (b) adaptive dc-link voltage control, and (c) adaptive dc-link voltage control with L_n at the first loading case. Fig. 14 illustrates that the adaptive dc voltage control scheme can reduce the switching noise ($\sim 20\% \downarrow$ in current ripple) compared with the fixed dc voltage case. Moreover, the adaptive dc-voltage-controlled LC-HAPF with L_n can further reduce the switching noise ($\sim 70\% \downarrow$ in current ripple). Fig. 15 shows the experimental neutral inverter currents i_{cn}, which also verifies the switching noise reduction by the adaptive dc-link voltage control and L_n.

Fig. 16(a) shows the performance comparison between the LC-HAPFs with and without L_n. With L_n case, its compensating current tracking ability can be enhanced; thus, the LC-HAPF can obtain a low THD_{isx} value under low $V_{dcU}, V_{dcL} = 25$ V. Without L_n case, a sufficient dc-link voltage (V_{dcU}, $V_{dcL} \geq 50$ V) should be applied to ensure its current tracking ability. To obtain a similar THD_{isx} value, the LC-HAPF with L_n can have a much lower dc operating voltage. In addition, the inverter power loss curve of LC-HAPF under different dc voltage levels is shown in Fig. 16(b). From Fig. 16(b), it clearly indicates that a lower inverter power loss can be obtained for the LC-HAPF with L_n.

For the adaptive dc-link voltage-controlled LC-HAPF with or without L_n, due to the fact that its reference dc voltage V^*_{dc} can be varied according to different loading conditions, its compensating performance will be influenced during each changing of the dc voltage level. Compared with the fixed dc voltage control, the adaptive dc control scheme will have

TABLE IX
EXPERIMENTAL RESULTS AFTER LC-HAPF COMPENSATION WITH ADAPTIVE DC-LINK VOLTAGE CONTROL AND L_N

After LC-HAPF Compensation with Adaptive DC-link Voltage Control and L_n								
Different Cases:		Q_{sxf} (var)	PF	THD_{isx} (%)	THD_{vx} (%)	i_{sx} (A_{rms})	i_{sn} (A_{rms})	V_{dcU}, V_{dcL}
1st inductive loading	A	-59.1	0.995	5.7	0.9	5.052	0.815	25V
	B	-88.3	0.994	5.9	0.9	5.011		
	C	-90.4	0.994	6.4	0.9	4.962		
1st and 2nd inductive loading	A	16.5	0.999	3.4	0.9	8.073	0.839	50V
	B	9.7	0.998	3.6	0.8	8.017		
	C	4.0	0.998	4.3	0.9	8.031		

TABLE X
EXPERIMENTAL INVERTER POWER LOSS OF LC-HAPF WITH FIXED V_{DCU}, $V_{DCL} = 75$ V, ADAPTIVE DC-LINK VOLTAGE CONTROL, AND ADAPTIVE DC-LINK VOLTAGE CONTROL WITH L_N

Inverter Power Loss of LC-HAPF		Fixed V_{dcU}, V_{dcL} = 75V	Adaptive DC	Adaptive DC with L_n
Power loss (W)	1st inductive loading	41W	37W (50V) ~10%↓	35W (25V) ~15%↓
	1st and 2nd inductive loading	59W	59W (75V)	54W (50V) ~9%↓

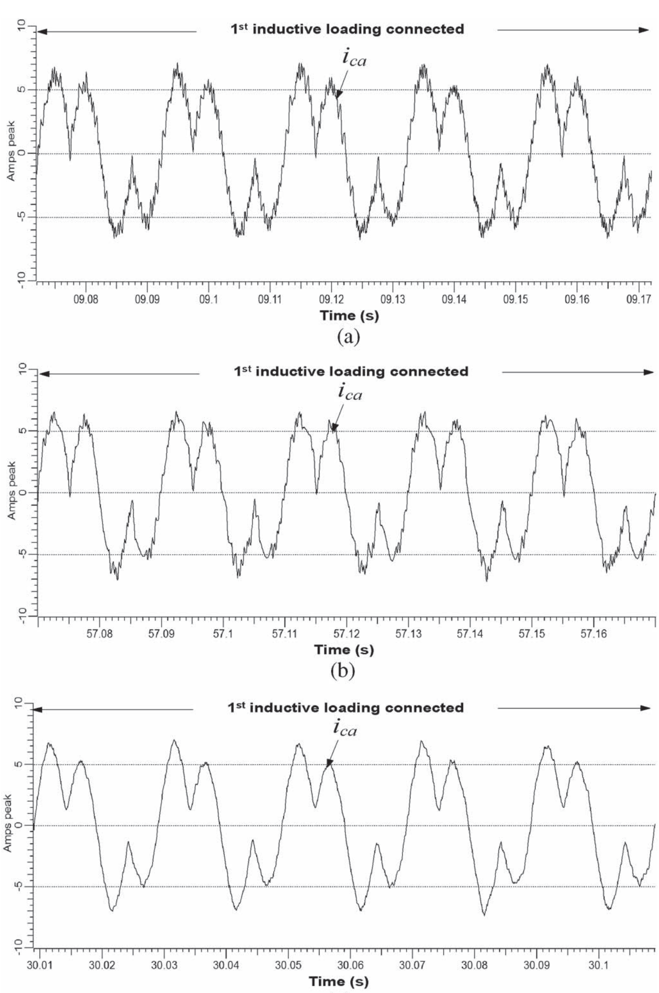

Fig. 14. Experimental i_{cx} of phase a with (a) a fixed V_{dcU}, $V_{dcL} = 75$ V, (b) adaptive dc-link voltage control, and (c) adaptive dc-link voltage control with L_n.

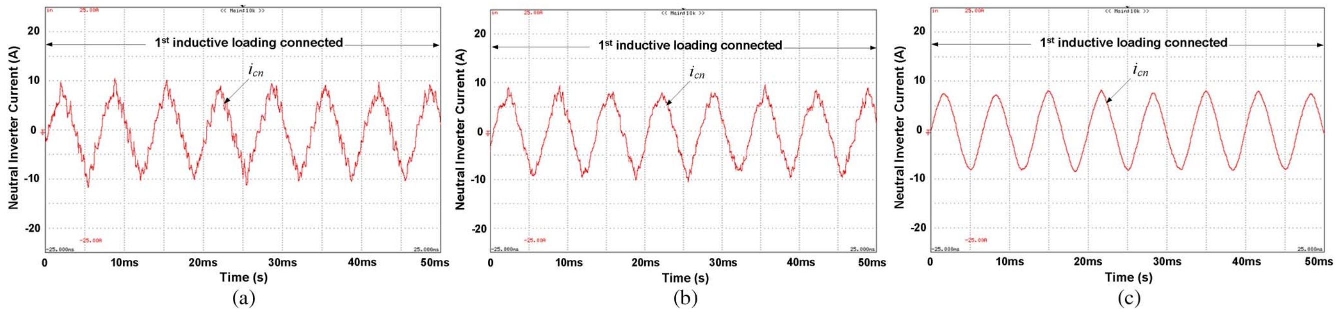

Fig. 15. Experimental i_{cn} with (a) a fixed $V_{\mathrm{dc}U}, V_{\mathrm{dc}L} = 75$ V, (b) adaptive dc-link voltage control, and (c) adaptive dc-link voltage control with L_n.

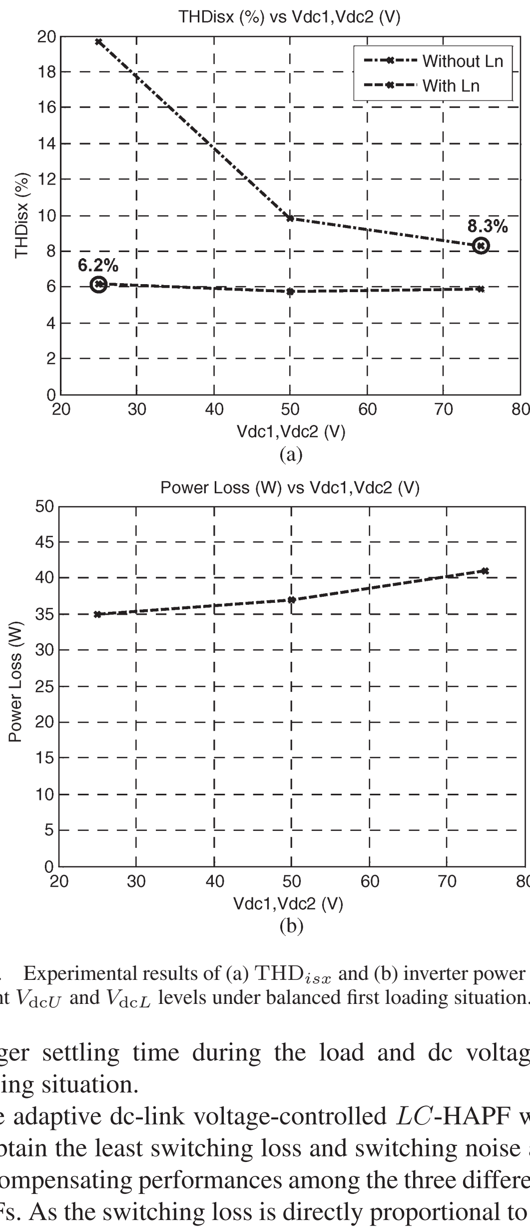

Fig. 16. Experimental results of (a) THD_{isx} and (b) inverter power loss with different $V_{\mathrm{dc}U}$ and $V_{\mathrm{dc}L}$ levels under balanced first loading situation.

a longer settling time during the load and dc voltage level changing situation.

The adaptive dc-link voltage-controlled LC-HAPF with L_n can obtain the least switching loss and switching noise and the best compensating performances among the three different LC-HAPFs. As the switching loss is directly proportional to the dc-link voltage and switching frequency indicated by (5), applying the fixed-frequency triangular PWM scheme will also yield the same trends of loss reduction results.

V. Conclusion

In this paper, an adaptive dc-link voltage-controlled LC-HAPF with a neutral inductor for both dynamic reactive power and current harmonic compensation in three-phase four-wire power systems has been proposed. Its dc controller's design procedures are discussed, so that the PI gain values can be designed accordingly. Moreover, the general design procedures for the adaptive dc-link voltage-controlled LC-HAPF with a neutral inductor are also given. Finally, a 220-V 10-kVA LC-HAPF laboratory prototype has been constructed and tested to verify the viability and effectiveness of the proposed solution, in which it can obtain the least switching loss and switching noise and the best compensating performances compared with the conventional fixed and newly adaptive dc LC-HAPF without neutral inductor. Moreover, it can significantly decrease the three-phase and neutral currents to enhance the power network efficiency.

References

[1] P. Salmerón and S. P. Litrán, "A control strategy for hybrid power filter to compensate four-wires three-phase systems," *IEEE Trans. Power Electron.*, vol. 25, no. 7, pp. 1923–1931, Jul. 2010.

[2] V. F. Corasaniti, M. B. Barbieri, P. L. Arnera, and M. I. Valla, "Hybrid active filter for reactive and harmonics compensation in a distribution network," *IEEE Trans. Ind. Electron.*, vol. 56, no. 3, pp. 670–677, Mar. 2009.

[3] D. Rivas, L. Moran, J. W. Dixon, and J. R. Espinoza, "Improving passive filter compensation performance with active techniques," *IEEE Trans. Ind. Electron.*, vol. 50, no. 1, pp. 161–170, Feb. 2003.

[4] V.-F. Corasaniti, M.-B. Barbieri, P.-L. Arnera, and M.-I. Valla, "Hybrid power filter to enhance power quality in a medium voltage distribution," *IEEE Trans. Ind. Electron.*, vol. 56, no. 8, pp. 2885–2893, Aug. 2009.

[5] A. Luo, X.-Y. Xu, L. Fang, H.-H. Fang, J.-B. Wu, and C.-P. Wu, "Feedback-feedforward PI-type iterative learning control strategy for hybrid active power filter with injection circuit," *IEEE Trans. Ind. Electron.*, vol. 57, no. 11, pp. 3767–3779, Nov. 2010.

[6] S. Rahmani, A. Hamadi, and K. Al-Haddad, "A Lyapunov-function-based control for a three-phase shunt hybrid active filter," *IEEE Trans. Ind. Electron.*, vol. 59, no. 3, pp. 1418–1429, Mar. 2012.

[7] H. Fujita, T. Yamasaki, and H. Akagi, "A hybrid active filter for damping of harmonic resonance in industrial power systems," *IEEE Trans. Power Electron.*, vol. 15, no. 2, pp. 215–222, Mar. 2000.

[8] W. Tangtheerajaroonwong, T. Hatada, K. Wada, and H. Akagi, "Design and performance of a transformerless shunt hybrid filter integrated into a three-phase diode rectifier," *IEEE Trans. Power Electron.*, vol. 22, no. 5, pp. 1882–1889, Sep. 2007.

[9] S. Rahmani, A. Hamadi, N. Mendalek, and K. Al-Haddad, "A new control technique for three-phase shunt hybrid power filter," *IEEE Trans. Ind. Electron.*, vol. 56, no. 8, pp. 2904–2915, Aug. 2009.

[10] A. Bhattacharya, C. Chakraborty, and S. Bhattacharya, "Parallel-connected shunt hybrid active power filters operating at different switching frequencies for improved performance," *IEEE Trans. Ind. Electron.*, vol. 59, no. 11, pp. 4007–4019, Nov. 2012.

[11] C.-S. Lam, W.-H. Choi, M.-C. Wong, and Y.-D. Han, "Adaptive DC-link voltage controlled hybrid active power filters for reactive power compensation," *IEEE Trans. Power Electron.*, vol. 27, no. 4, pp. 1758–1772, Apr. 2012.

[12] P. Rodriguez, J. I. Candela, A. Luna, L. Asiminoaei, R. Teodorescu, and F. Blaabjerg, “Current harmonics cancellation in three-phase four-wire systems by using a four-branch star filtering topology,” *IEEE Trans. Power Electron.*, vol. 24, no. 8, pp. 1939–1950, Aug. 2009.
[13] C.-S. Lam, X.-X. Cui, W.-H. Choi, M.-C. Wong, and Y.-D. Han, “Minimum inverter capacity design for three-phase four-wire LC-hybrid active power filters,” *IET Power Electron.*, vol. 5, no. 7, pp. 956–968, Aug. 2012.
[14] C.-S. Lam, M.-C. Wong, and Y.-D. Han, “Voltage swell and overvoltage compensation with unidirectional power flow controlled dynamic voltage restorer,” *IEEE Trans. Power Del.*, vol. 23, no. 4, pp. 2513–2521, Oct. 2008.
[15] M.-C. Wong, J. Tang, and Y.-D. Han, “Cylindrical coordinate control of three-dimensional PWM technique in three-phase four-wired trilevel inverter,” *IEEE Trans. Power Electron.*, vol. 18, no. 1, pp. 208–220, Jan. 2003.
[16] N.-Y. Dai and M.-C. Wong, “Design considerations of coupling inductance for active power filters,” in *Proc. 6th IEEE ICIEA*, Jun. 2011, pp. 1370–1375.
[17] V. Khadkikar, A. Chandra, and B. N. Singh, “Generalized single-phase p-q theory for active power filtering: Simulation and DSP-based experimental investigation,” *IET Power Electron.*, vol. 2, no. 1, pp. 67–78, Jan. 2009.
[18] L. H. Wu, F. Zhuo, P. B. Zhang, H. Y. Li, and Z. A. Wang, “Study on the influence of supply-voltage fluctuation on shunt active power filter,” *IEEE Trans. Power Del.*, vol. 22, no. 3, pp. 1743–1749, Jul. 2007.
[19] W.-H. Choi, C.-S. Lam, M.-C. Wong, and Y.-D. Han, “Analysis of DC-link voltage controls in three-phase four-wire hybrid active power filters,” *IEEE Trans. Power Electron.*, vol. 28, no. 5, pp. 2180–2191, May 2013.
[20] H. Akagi, S. Ogasawara, and K. Hyosung, “The theory of instantaneous power in three-phase four-wire systems: A comprehensive approach,” in *Conf. Rec. 34th IEEE IAS Annu. Meeting*, 1999, vol. 1, pp. 431–439.
[21] M. Aredes, J. Hafner, and K. Heumann, “Three-phase four-wire shunt active filter control strategies,” *IEEE Trans. Power Electron.*, vol. 12, no. 2, pp. 311–318, Mar. 1997.
[22] C.-S. Lam, M.-C. Wong, and Y.-D. Han, “Hysteresis current control of hybrid active power filters,” *IET Power Electron.*, vol. 5, no. 7, pp. 1175–1187, Aug. 2012.
[23] *IEEE Recommended Practices and Requirements for Harmonic Control in Electrical Power Systems*, IEEE Std. 519-1992, 1992.
[24] *Electromagnetic Compatibility (EMC), Part 3: Limits, Section 2: Limits for Harmonics Current Emissions*, IEC Std. 61000-3-2, 1997.
[25] *IEEE Recommended Practice on Monitoring Electric Power Quality*, IEEE Std. 1159, 1995.

Chi-Seng Lam (S’04–M’12) received the B.Sc., M.Sc., and Ph.D. degrees in electrical and electronics engineering from the University of Macau (UM), Macao, China, in 2003, 2006, and 2012, respectively.

From 2006 to 2009, he was an Electrical and Mechanical Engineer with the Campus Development and Engineering Section, UM. In 2013, he was a Postdoctoral Fellow with The Hong Kong Polytechnic University, Hong Kong. He is currently an Assistant Professor in the State Key Laboratory of Analog and Mixed-Signal VLSI, UM. He has coauthored more than 30 technical journal and conference papers. His research interests include integrated power electronics controllers, power electronics converters, energy saving, power quality compensators, smart grid technology, electric vehicle chargers, and renewable energy.

Dr. Lam was the recipient of the 3rd Regional Inter-University Postgraduate Electrical and Electronic Engineering Conference Merit Paper Award in 2005. He was also the recipient of the Macao Scientific and Technological R&D Award for Postgraduates (Ph.D. Level) in 2012.

Man-Chung Wong (SM’06) received the B.Sc. and M.Sc. degrees in electrical and electronics engineering from the University of Macau (UM), Macao, China, in 1993 and 1997, respectively, and the Ph.D. degree in electrical engineering from Tsinghua University, Beijing, China, in 2003.

Since 2008, he has been an Associate Professor with the Department of Electrical and Computer Engineering, Faculty of Science and Technology, UM. His research interests include renewable energy, power quality compensators, high-power electronic interfaces for utility systems, and flexible ac transmission systems.

Dr. Wong was the recipient of the Young Scientist Award from the “Insituto Internacional de Macau” in 2000, the Young Scholar Award from UM in 2001, the Second Prize of the 2003 Tsinghua University Excellent Ph.D. Thesis Award, and the Third Class Award in Technology Invention Award given by the Macao Scientific and Technological R&D Award in 2012.

Wai-Hei Choi (S’09) received the B.Sc. and M.Sc. degrees in electrical and electronics engineering from the University of Macau (UM), Macao, China, in 2009 and 2012, respectively.

He is currently a Research Assistant with the Power Electronics Laboratory, UM. His research interests focus on power electronics applications and power quality compensation.

Mr. Choi was the recipient of the Champion Award in the “Schneider Electric Energy Efficiency Cup,” Hong Kong, in 2010. He was also a recipient of the Second Prize of the 5th National University Students Social Practice and Science Contest on Energy Saving and Emission Reduction in 2012.

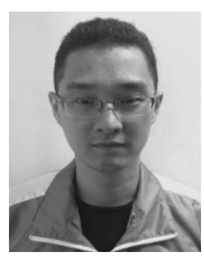

Xiao-Xi Cui received the B.Sc. degree in electronic and information engineering from Guangxi University, Nanning, China, in 2007 and the M.Sc. degree in electrical and electronics engineering from the University of Macau (UM), Macao, China, in 2012.

Since 2007, he has been with the Power Electronics Laboratory, UM, where he is currently a Research Assistant. His research interests include power electronics converters, energy saving, and power quality compensators.

Mr. Cui was a recipient of the Second Prize of the 5th National University Students Social Practice and Science Contest on Energy Saving and Emission Reduction in 2012.

Hong-Ming Mei was born in Hubei, China, in 1984. He received the B.Eng. degree in electrical engineering from Tsinghua University, Beijing, China, in 2007, where he is currently working toward the Ph.D. degree.

His research interests include high-power electronics, power quality compensation, flexible ac transmission systems, and applications of voltage-source-converter HVDC.

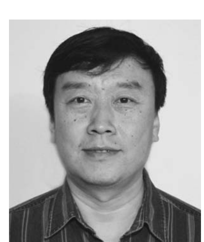

Jian-Zheng Liu was born in Harbin, China, in 1961. He received the B.Eng. and M.S. degrees in electrical engineering from Tsinghua University, Beijing, China, in 1985 and 1988, respectively.

Since 2000, he has been an Associate Professor with the Department of Electrical Engineering, Tsinghua University. His research interests include renewable energy, motor drives, high-power electronic interfaces for utility systems, and power quality compensation.